

SketchGuard: Scaling Byzantine-Robust Decentralized Federated Learning via Sketch-Based Screening

Murtaza Rangwala¹ Farag Azzedin^{1,2} Richard O. Sinnott¹ Rajkumar Buyya¹

Abstract

Decentralized Federated Learning enables privacy-preserving collaborative training without centralized servers but remains vulnerable to Byzantine attacks. Existing defenses require exchanging high-dimensional model vectors with all neighbors each round, creating prohibitive costs at scale. We propose SketchGuard, which decouples Byzantine filtering from aggregation via sketch-based screening. SketchGuard compresses d -dimensional models to k -dimensional sketches ($k \ll d$) using Count Sketch, then fetches full models only from accepted neighbors, reducing communication complexity from $O(d|\mathcal{N}_i|)$ to $O(k|\mathcal{N}_i| + d|\mathcal{S}_i|)$, where $|\mathcal{N}_i|$ is the neighbor count and $|\mathcal{S}_i| \leq |\mathcal{N}_i|$ is the accepted count. We prove convergence in strongly convex and non-convex settings, showing that approximation errors introduce only a $(1 + O(\epsilon))$ factor in the effective threshold. Experiments demonstrate SketchGuard maintains state-of-the-art robustness (mean TER deviation ≤ 0.5 percentage points) while reducing computation by up to 82% and communication by 50–70%.

1. Introduction

Federated Learning (FL) enables collaborative training of AI models over distributed data while preserving privacy by keeping raw data local (McMahan et al., 2017). However, the canonical, server-assisted architecture of FL centralizes aggregation of model parameters, creating a single point of failure, a communication bottleneck, and trust issues (Fang et al., 2024). These drawbacks have catalyzed Decentralized Federated Learning (DFL), where clients exchange model updates in a peer-to-peer manner over a dynamic

¹School of Computing and Information Systems, The University of Melbourne, Australia ²Department of Information and Computer Science, King Fahd University of Petroleum and Minerals, Dhahran, Saudi Arabia. Correspondence to: Murtaza Rangwala <rangwalam@unimelb.edu.au>.

Preprint. January 29, 2026.

communication graph, thereby improving scalability and resilience (Martínez Beltrán et al., 2023).

A central challenge in DFL is *byzantine robustness*: the ability to withstand malicious clients that submit arbitrary or carefully crafted updates to poison training, induce consensus drift, or trigger targeted failures (Blanchard et al., 2017; Baruch et al., 2019). Unlike centralized FL where robust rules such as Krum (Blanchard et al., 2017), coordinate-wise Median (Yin et al., 2018), or Trimmed-Mean (Wang et al., 2025) are applied once at a centralized server, DFL requires every client to aggregate its neighbors' updates under local, graph-limited views, often with non-IID data and time-varying connectivity. To address this added complexity, most DFL defenses adopt *local-consistency filters*, where clients accept a neighbor's update only if it is sufficiently similar to their own state, and then average over the accepted subset (Guo et al., 2022; He et al., 2022; Fang et al., 2024; Cajaraville-Aboy et al., 2025; El-Mhamdi et al., 2021). These mechanisms provide convergence and robustness guarantees in both strongly convex and non-convex model training settings, yet suffer from a fundamental scalability bottleneck: clients must exchange and compare complete, high-dimensional model vectors with all neighbors in every round. For emerging web-scale applications like decentralized training of frontier models with billions of parameters across thousands of distributed participants (Borzunov et al., 2023; Long, 2024), this creates prohibitive communication and computation costs that prevent practical implementation of these systems at scale.

Sketch-based compression offers tools for communication efficient learning. Count Sketch, for instance, compresses a vector of d dimensions into a summary of k dimensions using simple hash and sign functions, where $k \ll d$. Sketches are linear and allow approximate preservation of coordinates, thereby supporting fast similarity estimation with formal guarantees (Charikar et al., 2002; Rothchild et al., 2020; Gattani et al., 2024). While sketching has proven effective for bandwidth reduction in FL, extending it to *Byzantine-robust, fully decentralized aggregation*, where compressed representations must support secure neighbor screening, remains underexplored.

In this paper, we propose SKETCHGUARD, a general frame-

work for Byzantine-robust DFL that decouples filtering from aggregation through sketch-based neighbor screening. Our key insight is that similarity-based Byzantine filtering can operate on compressed representations, while the final aggregation requires full precision models only for accepted neighbors. SKETCHGUARD is applicable to any similarity-based Byzantine defense that relies on Euclidean distance measures (e.g., (Fang et al., 2024; He et al., 2022; Sun et al., 2024; Pillutla et al., 2022)), but for our theoretical analysis and empirical evaluation, we instantiate it with state-of-the-art BALANCE aggregation (Fang et al., 2024), which provides the strongest theoretical guarantees among existing methods. Our main contributions can be summarized as follows:

- We provide rigorous analysis showing that Count Sketch compression maintains Byzantine resilience with controlled degradation bounds.
- We establish convergence rates for SKETCHGUARD in both strongly convex and non-convex settings.
- Through comprehensive experiments across multiple datasets, network topologies, and attack scenarios, we demonstrate that our approach achieves identical robustness to state-of-the-art methods while reducing communication overhead by 50-70% and computation time by up to 82%.

2. Preliminaries and Related Work

This section provides technical background on DFL protocols, Byzantine attack models, and compression techniques, and discusses related work in each area.

2.1. DFL Problem Formulation and Protocol

Consider n clients connected by an undirected graph $G = (V, E)$, where each client $i \in V$ possesses a private dataset \mathcal{D}_i and maintains a local model $\mathbf{w}_i \in \mathbb{R}^d$. The collective objective is to minimize the average empirical loss:

$$\min_{\mathbf{w} \in \mathbb{R}^d} F(\mathbf{w}) = \frac{1}{n} \sum_{i=1}^n f_i(\mathbf{w}), \quad (1)$$

where $f_i(\mathbf{w}) = \mathbb{E}_{(\mathbf{x}, y) \sim \mathcal{D}_i} [\ell(\mathbf{w}; \mathbf{x}, y)]$ is the expected loss over client i 's data distribution.

The DFL protocol alternates between two phases. First, clients perform local updates:

$$\mathbf{w}_i^{t+1/2} = \mathbf{w}_i^t - \eta \nabla f_i(\mathbf{w}_i^t). \quad (2)$$

Then, each client aggregates neighbor models according to:

$$\mathbf{w}_i^{t+1} = \alpha \mathbf{w}_i^{t+1/2} + (1-\alpha) \cdot \text{AGG}_i \left(\{\mathbf{w}_j^{t+1/2} : j \in \mathcal{N}_i\} \right), \quad (3)$$

where \mathcal{N}_i denotes client i 's neighbors and AGG_i is a local aggregation function.

2.2. Byzantine Attack Models

We consider f -Byzantine adversaries that control up to f clients per neighborhood. Byzantine clients can deviate arbitrarily from the protocol, presenting a spectrum of threats ranging from simple disruption to sophisticated coordinated manipulation. These adversaries may employ model poisoning by sending crafted parameters $\hat{\mathbf{w}}_j$ designed to maximize deviation from honest updates while evading detection by robust aggregation rules. Representative attacks include random noise injection (Blanchard et al., 2017), data label flipping (Baruch et al., 2019), and gradient-based perturbation optimization (Muñoz González et al., 2017). More sophisticated adversaries operate adaptively, observing honest client behavior and adjusting their strategy accordingly. Such attacks (Fang et al., 2020; Shejwalkar & Houmansadr, 2021) solve optimization problems to craft maximally harmful updates that remain within detection thresholds of similarity-based defenses. The most challenging scenarios involve collusive attacks where multiple Byzantine clients coordinate their malicious behavior (Xie et al., 2020; Muñoz González et al., 2017), potentially overwhelming local robust aggregation mechanisms that assume independent adversarial actions. These coordinated strategies can amplify individual malicious impact through strategic cooperation, creating correlated deviations that may appear legitimate to individual clients with limited neighborhood views.

The fundamental challenge for DFL robustness lies in defending against these varied attack strategies under graph-limited visibility, where each client must make aggregation decisions based solely on local neighborhood information rather than global network state. This constraint makes similarity-based filtering particularly attractive, as it provides a principled approach to neighbor screening that remains effective across different attack types while being computationally tractable for individual clients.

2.3. Byzantine-Robust DFL Defenses

As explained in the previous section, existing DFL defenses have converged on similarity-based neighbor filtering as the dominant paradigm, with methods differing primarily in their filtering criteria and aggregation mechanisms.

UBAR (Guo et al., 2022) utilizes two-stage neighbor selection based on distance and loss filtering, followed by averaging.

LEARN (El-Mhamdi et al., 2021) employs multiple rounds of model exchanges per iteration with trimmed-mean aggregation. The multi-round communication exacerbates the pre-existing scalability issues with similarity-based filtering

mechanisms.

SCCLIP (He et al., 2022) applies self-centered clipping to each received neighbor model, mitigating large-magnitude deviations. It provides convergence guarantees in non-convex settings but also requires full model comparisons.

BALANCE (Fang et al., 2024) introduces adaptive similarity thresholds for neighbor screening with strong theoretical convergence guarantees in both strongly convex and non-convex settings. It achieves state-of-the-art robustness but at a high computational cost.

WFAGG (Cajaraville-Aboy et al., 2025) proposes multi-filter approaches for dynamic topologies, combining several screening mechanisms while maintaining the same computational complexity limitations.

However, all these methods require computation of similarities between complete d -dimensional model vectors with all neighbors, creating bottlenecks that prevent practical web-scale deployments. A detailed comparison of SKETCHGUARD with existing methods is provided in Appendix C.

2.4. Compression Techniques in FL

Communication and computational efficiency remain fundamental challenges in FL, motivating extensive research in model compression. Quantization techniques reduce parameter precision (Alistarh et al., 2017), sparsification methods transmit only significant updates (Stich et al., 2018; Sattler et al., 2020), and low-rank approaches exploit model structure (Konečný et al., 2016; Haddadpour et al., 2021). However, most compression techniques target benign settings and often compromise robustness when Byzantine participants are present. Traditional quantization can amplify malicious update impact, while sparsification enables attackers to concentrate influence in transmitted coordinates. More broadly, existing compression methods are incompatible with Byzantine-robust aggregation algorithms, preventing scalable deployment of robust FL.

2.5. Count Sketch

Count Sketch (Charikar et al., 2002) provides randomized linear projection with properties that make it particularly suitable for Byzantine-robust neighbor screening in DFL. Given $\mathbf{w} \in \mathbb{R}^d$, a Count Sketch of size $k \ll d$ is constructed using hash function $h : [d] \rightarrow [k]$ and sign function $s : [d] \rightarrow \{-1, +1\}$:

$$\text{CS}(\mathbf{w})[b] = \sum_{i:h(i)=b} s(i)w_i, \quad b = 1, \dots, k. \quad (4)$$

Count Sketch possesses three critical properties for robust DFL screening. First, linearity ensures consistent compression across clients, as $\text{CS}(\alpha\mathbf{u} + \beta\mathbf{v}) = \alpha\text{CS}(\mathbf{u}) + \beta\text{CS}(\mathbf{v})$.

Second, unbiased coordinate estimation provides formal recovery guarantees (Charikar et al., 2002; Rothchild et al., 2020). Third, and most crucial for similarity-based Byzantine filtering, Count Sketch preserves approximate Euclidean distances:

Lemma 2.1 (Distance Preservation (Charikar et al., 2002)). *For any vectors $\mathbf{u}, \mathbf{v} \in \mathbb{R}^d$ and sketch size $k = O(\epsilon^{-2} \log(1/\delta))$, with probability at least $1 - \delta$:*

$$(1 - \epsilon)\|\mathbf{u} - \mathbf{v}\|^2 \leq \|\text{CS}(\mathbf{u}) - \text{CS}(\mathbf{v})\|^2 \leq (1 + \epsilon)\|\mathbf{u} - \mathbf{v}\|^2 \quad (5)$$

3. SketchGuard: Scalable Robust Aggregation

We now present SKETCHGUARD, which leverages Lemma 2.1 to perform neighbor screening in the sketch domain. The key design rationale is that if Count Sketch approximately preserves distances, then similarity-based filtering decisions made using sketches will closely match those made using full-precision models, allowing us to defer expensive full-model exchanges until after filtering.

3.1. Protocol Description

At each DFL training round t , client i executes the four-phase SKETCHGUARD protocol detailed in Algorithm 1 and illustrated in Figure 1 as follows:

Phase 1: Local Training. Client i performs local stochastic gradient descent as shown in Equation 2.

Phase 2: Sketch Exchange. The updated model is compressed using $\text{CS}(\mathbf{s}_i^{t+1/2}) = \text{CS}(\mathbf{w}_i^{t+1/2})$, and these k -dimensional sketches are exchanged with the immediate neighbors \mathcal{N}_i .

Phase 3: Adaptive Filtering. Neighbor j is accepted if their sketch distance satisfies:

$$\|\mathbf{s}_i^{t+1/2} - \mathbf{s}_j^{t+1/2}\| \leq \gamma \exp(-\kappa t/T) \|\mathbf{s}_i^{t+1/2}\| \quad (6)$$

where γ controls the base threshold, κ the decay rate, and T the total rounds. This adaptive threshold mechanism is adopted from BALANCE (Fang et al., 2024), where the exponential decay reflects convergence of honest clients over time.

Remark 3.1. When using Count Sketch compression with approximation parameter ϵ , the effective threshold parameter becomes $\gamma_{\text{eff}} = \gamma \sqrt{(1 + \epsilon)/(1 - \epsilon)}$ to account for distance preservation errors in the sketch domain, as established by the analysis in Lemma 2.1. This ensures that our theoretical convergence guarantees in Section 4 accurately reflect the impact of compression on filtering decisions.

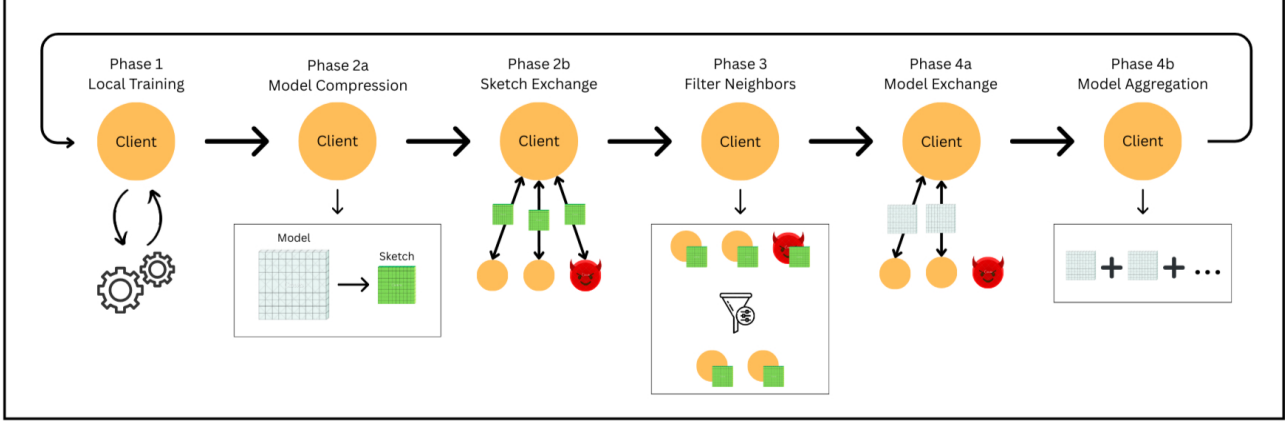


Figure 1. The SketchGuard Protocol

Phase 4: Model Aggregation. Full models are fetched from accepted neighbors \mathcal{S}_i^t . Before aggregation, each received model $\mathbf{w}_j^{t+1/2}$ is verified by recomputing its sketch and comparing with the originally received $\mathbf{s}_j^{t+1/2}$. Any neighbor whose model fails verification is removed from \mathcal{S}_i^t . The verified models are then aggregated:

$$\mathbf{w}_i^{t+1} = \alpha \mathbf{w}_i^{t+1/2} + \frac{(1-\alpha)}{|\mathcal{S}_i^t|} \sum_{j \in \mathcal{S}_i^t} \mathbf{w}_j^{t+1/2} \quad (7)$$

where $\alpha \in [0, 1]$ balances self-reliance and collaboration.

Algorithm 1 SKETCHGUARD: Robust Aggregation via Adaptive Sketch-Based Filtering

Require: Local data \mathcal{D}_i , neighbors \mathcal{N}_i , parameters γ, κ, α , sketch size k

Ensure: Updated model \mathbf{w}_i^{t+1}

- 1: $\mathbf{w}_i^{t+1/2} \leftarrow \mathbf{w}_i^t - \eta \mathbf{g}(\mathbf{w}_i^t)$
- 2: $\mathbf{s}_i^{t+1/2} \leftarrow \text{CS}(\mathbf{w}_i^{t+1/2})$
- 3: Exchange sketches $\mathbf{s}_i^{t+1/2}$ with neighbors \mathcal{N}_i
- 4: $\tau \leftarrow \gamma \exp(-\kappa T/T) \|\mathbf{s}_i^{t+1/2}\|$
- 5: $\mathcal{S}_i^t \leftarrow \{j \in \mathcal{N}_i : \|\mathbf{s}_i^{t+1/2} - \mathbf{s}_j^{t+1/2}\| \leq \tau\}$
- 6: **if** $|\mathcal{S}_i^t| = 0$ and $|\mathcal{N}_i| > 0$ **then**
- 7: $\mathcal{S}_i^t \leftarrow \{\arg \min_{j \in \mathcal{N}_i} \|\mathbf{s}_i^{t+1/2} - \mathbf{s}_j^{t+1/2}\|\}$
- 8: **end if**
- 9: Fetch models $\{\mathbf{w}_j^{t+1/2}\}_{j \in \mathcal{S}_i^t}$ from accepted neighbors
- 10: Verify $\text{CS}(\mathbf{w}_j^{t+1/2}) = \mathbf{s}_j^{t+1/2}$ for each $j \in \mathcal{S}_i^t$; remove if mismatch
- 11: $\mathbf{w}_i^{t+1} \leftarrow \alpha \mathbf{w}_i^{t+1/2} + \frac{1-\alpha}{|\mathcal{S}_i^t|} \sum_{j \in \mathcal{S}_i^t} \mathbf{w}_j^{t+1/2}$
- 12: **return** \mathbf{w}_i^{t+1}

3.2. Complexity Analysis and Performance Trade-offs

We analyze the per-node-per-round complexity of SKETCHGUARD compared to the best-case computation and communication complexity of existing Byzantine-robust methods.

Let d denote the model dimension, $|\mathcal{N}_i|$ the number of neighbors, k the sketch size, and $|\mathcal{S}_i^t|$ the number of accepted neighbors. For computational complexity, SKETCHGUARD executes four phases per round:

- Sketch generation: $O(d)$
- Neighbor screening (compressed domain): $O(k \cdot |\mathcal{N}_i|)$
- Model verification & aggregation (accepted neighbors): $O(d \cdot |\mathcal{S}_i^t|)$

This yields total complexity $O(d + k \cdot |\mathcal{N}_i| + d \cdot |\mathcal{S}_i^t|)$, compared to $O(d \cdot |\mathcal{N}_i|)$ for traditional methods that perform full-precision screening of all neighbors.

For communication complexity, SKETCHGUARD transmits two types of messages: sketches to all neighbors and full models to accepted neighbors. This results in $O(k \cdot |\mathcal{N}_i| + d \cdot |\mathcal{S}_i^t|)$ parameters per round, compared to $O(d \cdot |\mathcal{N}_i|)$ for existing approaches.

The theoretical requirement $k = O(\epsilon^{-2} \log(1/\delta))$ translates to practical sketch sizes that remain much smaller than model dimensions while providing strong approximation guarantees. SKETCHGUARD's performance benefits scale with three factors: (1) the compression ratio d/k , where larger models yield greater savings, (2) the filtering effectiveness ratio $|\mathcal{S}_i^t|/|\mathcal{N}_i|$, where successful Byzantine rejection reduces the number of full models fetched, and (3) network degree $|\mathcal{N}_i|$, where denser connectivity amplifies the screening overhead reduced by compression. While sketch generation and exchange introduce $O(d + k \cdot |\mathcal{N}_i|)$ overhead even in benign settings, this cost becomes negligible as model dimensionality and network scale increase, which characterizes the web-scale deployments where Byzantine robustness is necessary.

Table 1. Computational complexity comparison with state-of-the-art (SOTA) across training phases.

Training Phase	SOTA	SketchGuard
Local Training	$O(d)$	$O(d)$
Sketch Generation	—	$O(d)$
Neighbor Screening	$O(d \cdot \mathcal{N}_i)$	$O(k \cdot \mathcal{N}_i)$
Model Verification & Aggregation	$O(d \cdot \mathcal{S}_i^t)$	$O(d \cdot \mathcal{S}_i^t)$
Total Per Round	$O(d + d \cdot \mathcal{N}_i + d \cdot \mathcal{S}_i^t)$	$O(d + k \cdot \mathcal{N}_i + d \cdot \mathcal{S}_i^t)$

4. Convergence Analysis

In this section, we establish that SKETCHGUARD maintains convergence guarantees despite compressed filtering by proving that sketch-based screening preserves the robustness properties of full-precision similarity-based defenses with controlled degradation bounds.

4.1. Technical Assumptions

We state the standard assumptions that impact on convergence analysis.

Assumption 4.1 (Strong Convexity). The population risk $F(\mathbf{w})$ is μ -strongly convex, i.e., for all $\mathbf{w}_1, \mathbf{w}_2 \in \Theta$, one has that:

$$F(\mathbf{w}_1) + \langle \nabla F(\mathbf{w}_1), \mathbf{w}_2 - \mathbf{w}_1 \rangle + \frac{\mu}{2} \|\mathbf{w}_2 - \mathbf{w}_1\|^2 \leq F(\mathbf{w}_2).$$

Assumption 4.2 (Smoothness). The population risk $F(\mathbf{w})$ is L -smooth, i.e., for all $\mathbf{w}_1, \mathbf{w}_2 \in \Theta$, we have that:

$$\|\nabla F(\mathbf{w}_1) - \nabla F(\mathbf{w}_2)\| \leq L \|\mathbf{w}_1 - \mathbf{w}_2\|.$$

Assumption 4.3 (Bounded Variance). The stochastic gradient $\mathbf{g}(\mathbf{w}_i)$ computed by an honest client $i \in \mathcal{H}$ is an unbiased estimator of the true gradient, and $\mathbf{g}(\mathbf{w}_i)$ has bounded variance, where \mathcal{H} is the set of honest clients. That is, $\forall i \in \mathcal{H}$, one has that:

$$\mathbb{E}[\mathbf{g}(\mathbf{w}_i)] = \nabla F(\mathbf{w}_i), \quad \mathbb{E}[\|\mathbf{g}(\mathbf{w}_i) - \nabla F(\mathbf{w}_i)\|^2] \leq \delta^2.$$

Assumption 4.4 (Bounded Parameters). For any honest client $i \in \mathcal{H}$, the model \mathbf{w}_i and $\|\nabla F(\mathbf{w}_i)\|$ are bounded. That is, $\forall i \in \mathcal{H}$, we have $\|\mathbf{w}_i\| \leq \psi$, and $\|\nabla F(\mathbf{w}_i)\| \leq \rho$.

Assumption 4.5 (Graph Connectivity). The subgraph induced by honest clients $G_{\mathcal{H}}$ remains connected throughout training.

Assumption 4.6 (Hash Function Synchronization). All clients use identical hash and sign functions for consistent sketching across the network. This is trivially satisfied by seeding the hash functions with the model's parameter count d , which is implicitly shared among all clients training the same architecture.

4.2. Main Convergence Results

Leveraging Lemma 2.1, we establish convergence guarantees for SKETCHGUARD that achieve similar results to those based on full-precision methods.

Theorem 4.7 (Strongly Convex Convergence with Compression). *For μ -strongly convex and L -smooth objectives, with learning rate $\eta \leq \min\{1/(4L), 1/\mu\}$ and effective threshold parameter $\gamma_{\text{eff}} = \gamma\sqrt{(1+\epsilon)/(1-\epsilon)}$, after T rounds:*

$$\begin{aligned} \mathbb{E}[F(\mathbf{w}_i^T) - F(\mathbf{w}^*)] &\leq (1 - \mu\eta)^T [F(\mathbf{w}_i^0) - F(\mathbf{w}^*)] \\ &\quad + \frac{2L\eta\delta^2}{\mu} + \frac{2\gamma_{\text{eff}}\rho\psi(1-\alpha)}{\mu\eta} \end{aligned} \quad (8)$$

where the compression error manifests only through the $(1+\epsilon)/(1-\epsilon)$ factor in γ_{eff} .

Proof. See Appendix A. \square

Theorem 4.8 (Non-Convex Convergence with Compression). *For non-convex L -smooth objectives, with the same parameter choices:*

$$\begin{aligned} \frac{1}{T} \sum_{t=0}^{T-1} \mathbb{E}[\|\nabla F(\mathbf{w}_i^t)\|^2] &\leq \frac{2[F(\mathbf{w}_i^0) - F^*]}{\eta T} \\ &\quad + 4L\eta\delta^2 + \frac{4\gamma_{\text{eff}}\rho\psi(1-\alpha)}{\eta} \end{aligned} \quad (9)$$

Proof. See Appendix B. \square

Both theorems demonstrate that SKETCHGUARD achieves optimal convergence rates for their respective settings (Garrigos & Gower, 2023), with sketch approximation introducing only a $(1 + O(\epsilon))$ multiplicative factor on the threshold-dependent terms in the convergence bounds. For practical values of ϵ (e.g., $\epsilon = 0.1$ yields $\gamma_{\text{eff}} \approx 1.1\gamma$), this degradation is minimal while enabling substantial compression.

4.3. Robustness Preservation Under Compression

Our final theoretical result establishes that sketch compression preserves Byzantine robustness guarantees with controlled degradation.

Lemma 4.9 (Sketch Compression Preserves Byzantine Resilience). *Under the conditions of Theorems 4.7 and 4.8, sketch-based filtering with effective threshold $\gamma_{\text{eff}} = \gamma\sqrt{(1+\epsilon)/(1-\epsilon)}$ provides equivalent Byzantine resilience to full-precision filtering with threshold γ_{eff} . Specifically, compression does not create new attack vectors beyond the controlled threshold degradation.*

Proof. This follows directly from the convergence analysis in Theorems 4.7 and 4.8. Both proofs bound the neighbor difference terms under sketch-based filtering (Appendix A.5):

$$\left\| \frac{1}{|\mathcal{S}_i|} \sum_{j \in \mathcal{S}_i} (\mathbf{w}_j^{t+1/2} - \mathbf{w}_i^{t+1/2}) \right\| \leq \gamma_{\text{eff}} \psi$$

This bound is identical in form to the full-precision case, differing only in the threshold parameter $\gamma \rightarrow \gamma_{\text{eff}}$. Since the convergence proofs do not require any additional structural assumptions about the filtering mechanism beyond this bound, any Byzantine strategy must satisfy the same constraints as in the full-precision case, but with the relaxed threshold γ_{eff} . Therefore, compression preserves the Byzantine resilience properties established by (Fang et al., 2024), with degradation bounded by the factor $\sqrt{(1+\epsilon)/(1-\epsilon)} = 1 + O(\epsilon)$. \square

5. Performance Evaluation

We evaluate SKETCHGUARD¹ through comprehensive experiments demonstrating that sketch-based compression maintains identical Byzantine robustness to state-of-the-art full-precision defenses while substantially reducing computational and communication overhead.

5.1. Experimental Setup

5.1.1. DATASETS AND MODELS

We evaluate on three federated learning benchmarks from the LEAF suite (Caldas et al., 2019): FEMNIST (62-class character recognition, 3,550 users, CNN with 6.6M parameters), CelebA (binary smile classification, 9,343 users, CNN with 2.2M parameters), and Sent140 (Twitter sentiment analysis, 660,120 users, LSTM with 1.2M parameters). These datasets provide naturally non-IID distributions reflecting real-world federated heterogeneity across both image and text modalities. Complete architectural specifications are provided in Appendix D.1.

¹Code and experiment artifacts available at [Anonymized Repository].

5.1.2. NETWORK TOPOLOGIES

We evaluate five topologies spanning from minimal connectivity (Ring, degree 2) to maximum connectivity (Fully Connected), with three intermediate Erdős-Rényi densities ($p \in \{0.2, 0.45, 0.6\}$). The Erdős-Rényi topologies are implemented as dynamic networks where connections are resampled after each round, modeling realistic peer-to-peer environments with changing connectivity. Robustness experiments use 20-node networks; scalability experiments use k-regular graphs scaling from 20 to 300 nodes, ensuring uniform node degree to isolate algorithmic scaling behavior from network topology effects. Complete specifications are in Appendix D.3.1.

5.1.3. ATTACK MODELS AND EVALUATION METRICS

We evaluate four attack strategies: Directed Deviation (Fang et al., 2020), an optimization-based attack maximizing deviation opposite to honest gradients; Gaussian (Blanchard et al., 2017), injecting random noise sampled from the Gaussian distribution; Krum (Fang et al., 2020), exploiting distance-based selection via clustered malicious models; and Backdoor (Bagdasaryan et al., 2020), embedding hidden trigger patterns for targeted misclassification. We vary Byzantine fraction from 0% to 80%. Detailed attack descriptions are in Appendix D.4. We report Test Error Rate (TER) for robustness, Attack Success Rate (ASR) for backdoor resilience, per-round computation time, and communication overhead. The details of these metrics are in Appendix D.2.

5.1.4. BASELINES AND CONFIGURATION

We compare against D-FedAvg (Lian et al., 2017), KRUM (Blanchard et al., 2017), UBAR (Guo et al., 2022), and BALANCE (Fang et al., 2024). We use sketch sizes $k = 1000$ (FEMNIST), $k = 350$ (CelebA), and $k = 180$ (Sent140), maintaining compression ratios of approximately 6600:1 with $\epsilon \lesssim 0.2$. All experiments use 10 global rounds, 3 local epochs, and 3 random seeds. Complete hyperparameters are in Appendix D.3.2.

5.2. Byzantine Robustness Evaluation

Figure 2 evaluates whether sketch-based compression degrades Byzantine robustness compared to full-precision defenses. Across all four attack types on FEMNIST, CelebA, and Sent140 datasets, SKETCHGUARD maintains robustness statistically indistinguishable from BALANCE and UBAR, with mean absolute TER deviation of only 0.38 percentage points versus BALANCE and 0.50 percentage points versus UBAR. This confirms that Count Sketch’s distance preservation properties (Lemma 2.1) translate to equivalent filtering decisions in practice.

Against directed deviation and Krum attacks, all three

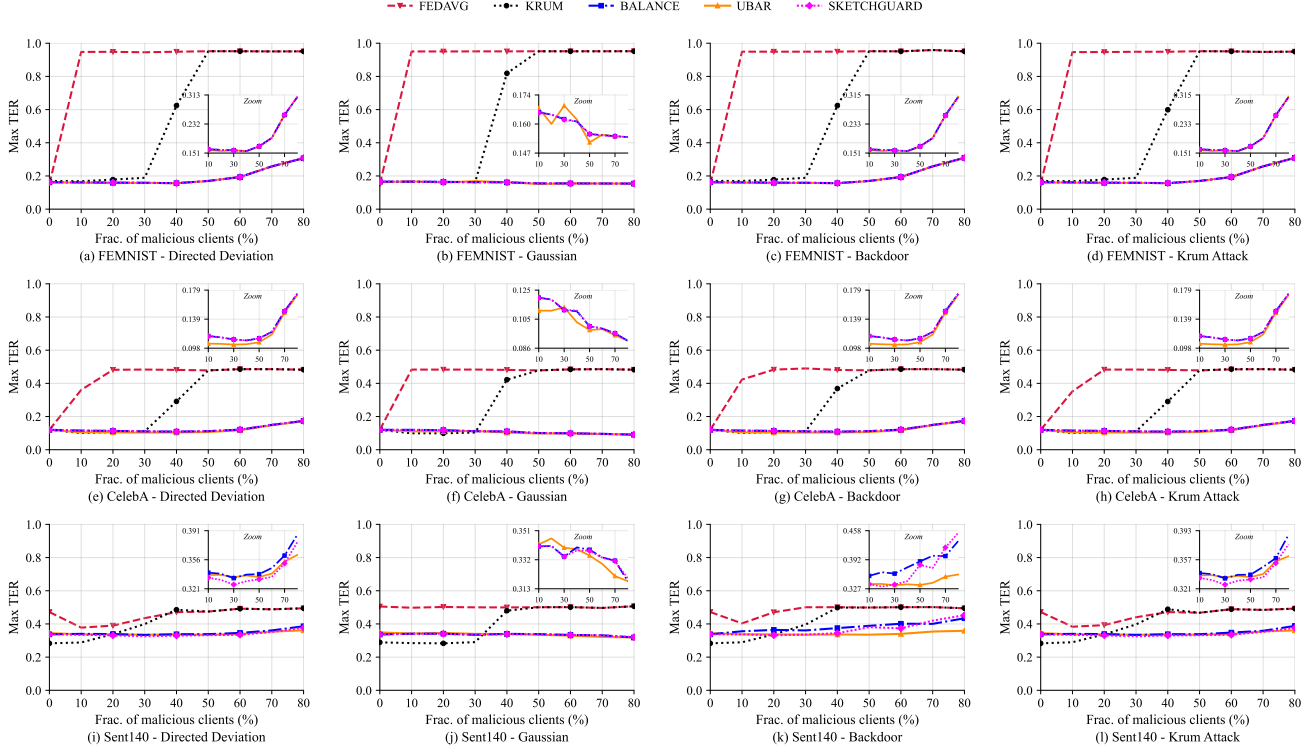


Figure 2. Impact of fraction of malicious clients on TER across different datasets and attack types. SKETCHGUARD maintains robustness equivalent to full-precision methods BALANCE and UBAR despite operating on compressed representations.

similarity-based methods (BALANCE, UBAR, SKETCHGUARD) maintain TER below 20% on FEMNIST and below 13% on CelebA even at 80% Byzantine clients, while D-FedAvg and KRUML collapse to near-random accuracy (TER > 60%). The Krum defense fails against its targeted attack (TER > 60% at 30%+ Byzantine), whereas similarity-based filtering—whether on full models or sketches—remains effective. For Gaussian attacks, SKETCHGUARD matches BALANCE within 0.03 percentage points on average.

For backdoor attacks, **SKETCHGUARD** achieves ASR comparable to **BALANCE** and **UBAR** across all datasets. On **FEMNIST**, all three methods achieve low ASR (6.98–9.94%), demonstrating that similarity-based filtering effectively identifies the scaled model updates characteristic of backdoor attacks. On **CelebA** and **Sent140**, all robust methods substantially outperform **D-FedAvg**. These results confirm that sketch compression does not create vulnerabilities to backdoor attacks.

5.3. Computational Efficiency

Having established that **SKETCHGUARD** matches state-of-the-art robustness, we now demonstrate the efficiency gains that motivate sketch-based filtering. Figure 3 evaluates computational scaling on FEMNIST with 50% Byzantine clients under directed deviation attacks.

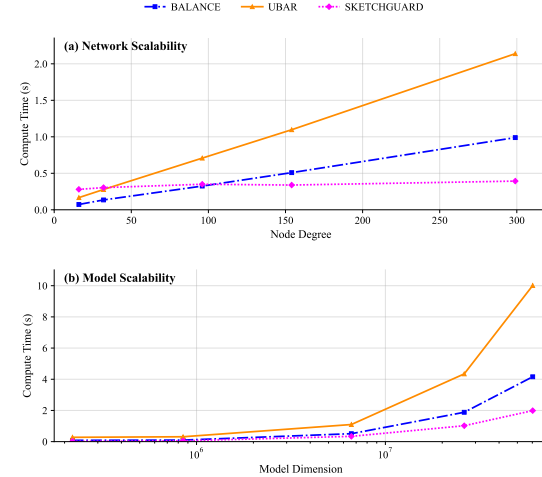


Figure 3. Impact of network size and model dimensionality on per-node computation time. SKETCHGUARD achieves substantial savings while maintaining equivalent robustness (Section 5.2).

SKETCHGUARD exhibits near-constant cost as network connectivity increases from 16 to 299 neighbors (Figure 3a), averaging 0.35s per round, while **BALANCE** and **UBAR** scale linearly. At 299 neighbors, **SKETCHGUARD** achieves 60% savings versus **BALANCE** (0.39s vs 0.99s) and 82% versus **UBAR** (0.39s vs 2.14s). This advantage grows with network density because sketch comparisons cost $O(k)$ per

neighbor versus $O(d)$ for full-precision methods.

For model dimensionality scaling (Figure 3b), SKETCHGUARD demonstrates sub-linear growth from 220K to 60M parameters, while BALANCE and UBAR scale linearly. At 60M parameters, SKETCHGUARD requires 2.0s versus 4.2s (BALANCE) and 10.0s (UBAR)—52% and 80% reductions. This sub-linear scaling emerges because sketch size k depends on approximation parameters (ϵ, δ) rather than model dimension d , making SKETCHGUARD increasingly valuable as models grow toward billion-parameter scales (Borzunov et al., 2023).

5.4. Communication Efficiency

SKETCHGUARD reduces per-round communication from $O(d|\mathcal{N}_i|)$ to $O(k|\mathcal{N}_i| + d|\mathcal{S}_i|)$, where $|\mathcal{S}_i| \leq |\mathcal{N}_i|$ is the accepted neighbor count. With compression ratios of approximately 6600:1, sketch overhead is negligible (<0.02% in benign settings). When Byzantine filtering rejects 50–70% of neighbors, communication reductions of 50–70% follow directly. These savings scale multiplicatively with model size and network connectivity, addressing the fundamental scalability bottleneck that has limited practical deployment of Byzantine-robust DFL.

5.5. Sensitivity Analysis

5.5.1. SKETCH SIZE ROBUSTNESS

A practical concern for sketch-based methods is sensitivity to the sketch size parameter k . SKETCHGUARD demonstrates remarkable insensitivity: across k values ranging from 500 to 100,000 on both FEMNIST and CelebA under 50% Byzantine clients with directed deviation attacks, TER remains completely stable (15.59% for FEMNIST, 10.35% for CelebA). Even at compression ratios exceeding 13,000:1 ($k = 500$ for FEMNIST’s 6.6M parameters), robustness is fully preserved. This insensitivity stems from Count Sketch’s distance preservation guarantees: sketch-based distances remain sufficiently accurate to distinguish Byzantine updates from honest behavior across a wide range of compression levels.

5.5.2. TOPOLOGY ROBUSTNESS

Table 2 presents robustness across five network topologies for the three similarity-based methods (non-robust D-FedAvg and KSUM consistently fail at $\sim 63\%$ TER as shown in Figure 2). SKETCHGUARD matches BALANCE across all topologies, confirming that sketch compression does not interact negatively with network structure. In well-connected topologies (ER $p \geq 0.45$, Fully Connected), all methods maintain TER below 20% even at 80% Byzantine. In sparse Ring topology, all methods exhibit graceful degradation at 60%+ attack intensity due to limited honest

Table 2. Test Error Rate (%) across topologies for robust methods, averaged over datasets and attacks (excl. backdoor).

Topology	Byz. %	UBAR	BALANCE	SG
Ring	20	19.0	19.9	19.9
	40	18.9	19.8	19.6
	60	30.2	30.6	30.3
	80	64.3	63.7	64.2
ER ($p=0.2$)	20	20.6	20.8	20.7
	40	20.2	20.4	20.3
	60	19.4	19.8	19.7
	80	18.8	20.4	20.0
ER ($p=0.45$)	20	20.1	20.4	20.3
	40	20.4	20.1	19.9
	60	19.6	19.8	19.5
	80	19.2	20.3	20.2
ER ($p=0.6$)	20	20.1	20.6	20.3
	40	20.1	20.2	20.1
	60	19.7	19.7	19.5
	80	19.1	19.2	19.0
Fully Conn.	20	20.0	20.5	20.3
	40	19.9	20.1	19.9
	60	19.5	19.7	19.5
	80	19.1	19.3	18.8

neighbors—a fundamental limitation of local aggregation rather than any method-specific weakness.

6. Conclusions

We proposed SKETCHGUARD, a framework for scaling Byzantine-robust decentralized federated learning through sketch-based neighbor screening. By decoupling filtering from aggregation, our approach reduces communication complexity from $O(d|\mathcal{N}_i|)$ to $O(k|\mathcal{N}_i| + d|\mathcal{S}_i|)$ while preserving the robustness guarantees of full-precision defenses.

Our theoretical analysis establishes that Count Sketch compression maintains Byzantine resilience with controlled degradation bounds, introducing only a $(1 + O(\epsilon))$ factor in the effective threshold. Experiments confirm that SKETCHGUARD matches state-of-the-art robustness (mean TER deviation ≤ 0.5 percentage points) while reducing computation by up to 82% and communication by 50–70% under typical attack scenarios.

Impact Statement

This paper presents work whose goal is to advance the field of Distributed Machine Learning. There are many potential societal consequences of our work, none of which we feel must be specifically highlighted here.

References

Alistarh, D., Grubic, D., Li, J., Tomioka, R., and Vojnovic, M. Qsgd: Communication-efficient sgd via gradient quantization and encoding. In *Advances in Neural Information Processing Systems*, volume 30. Curran Associates, Inc., 2017.

Bagdasaryan, E., Veit, A., Hua, Y., Estrin, D., and Shmatikov, V. How to backdoor federated learning. In *Proceedings of the Twenty Third International Conference on Artificial Intelligence and Statistics*, volume 108 of *Proceedings of Machine Learning Research*, pp. 2938–2948. PMLR, 26–28 Aug 2020.

Baruch, G., Baruch, M., and Goldberg, Y. A little is enough: Circumventing defenses for distributed learning. In *Advances in Neural Information Processing Systems*, volume 32. Curran Associates, Inc., 2019.

Blanchard, P., El Mhamdi, E. M., Guerraoui, R., and Stainer, J. Machine learning with adversaries: Byzantine tolerant gradient descent. In *Advances in Neural Information Processing Systems*, volume 30. Curran Associates, Inc., 2017.

Borzunov, A., Ryabinin, M., Chumachenko, A., Baranchuk, D., Dettmers, T., Belkada, Y., Samygin, P., and Raffel, C. A. Distributed inference and fine-tuning of large language models over the internet. In *Advances in Neural Information Processing Systems*, volume 36, pp. 12312–12331. Curran Associates, Inc., 2023.

Cajaraville-Aboy, D., Fernández-Vilas, A., Díaz-Redondo, R. P., and Fernández-Veiga, M. Byzantine-robust aggregation for securing decentralized federated learning. *IEEE Access*, 13:190947–190963, 2025.

Caldas, S., Duddu, S. M. K., Wu, P., Li, T., Konečný, J., McMahan, H. B., Smith, V., and Talwalkar, A. LEAF: A benchmark for federated settings. In *Workshop on Federated Learning for Data Privacy and Confidentiality*, 2019.

Charikar, M., Chen, K., and Farach-Colton, M. Finding frequent items in data streams. In Widmayer, P., Eidenbenz, S., Triguero, F., Morales, R., Conejo, R., and Hennessy, M. (eds.), *Automata, Languages and Programming*, pp. 693–703. Springer Berlin Heidelberg, 2002.

El-Mhamdi, E. M., Farhadkhani, S., Guerraoui, R., Guirguis, A., Hoang, L.-N., and Rouault, S. Collaborative learning in the jungle (decentralized, byzantine, heterogeneous, asynchronous and nonconvex learning). In *Advances in Neural Information Processing Systems*, volume 34, pp. 25044–25057. Curran Associates, Inc., 2021.

Fang, M., Cao, X., Jia, J., and Gong, N. Local model poisoning attacks to Byzantine-Robust federated learning. In *29th USENIX Security Symposium (USENIX Security 20)*, pp. 1605–1622. USENIX Association, August 2020.

Fang, M., Zhang, Z., Hairi, Khanduri, P., Liu, J., Lu, S., Liu, Y., and Gong, N. Byzantine-robust decentralized federated learning. In *Proceedings of the 2024 on ACM SIGSAC Conference on Computer and Communications Security*, CCS ’24, pp. 2874–2888. Association for Computing Machinery, 2024.

Garrigos, G. and Gower, R. M. Handbook of convergence theorems for (stochastic) gradient methods. *arXiv preprint arXiv:2301.11235*, 2023.

Gattani, V. S., Zhang, J., and Dasarathy, G. Communication-efficient federated learning over wireless channels via gradient sketching. *arXiv preprint arXiv:2410.23424*, 2024.

Guo, S., Zhang, T., Yu, H., Xie, X., Ma, L., Xiang, T., and Liu, Y. Byzantine-resilient decentralized stochastic gradient descent. *IEEE Transactions on Circuits and Systems for Video Technology*, 32(6):4096–4106, 2022. doi: 10.1109/TCSVT.2021.3116976.

Haddadpour, F., Kamani, M. M., Mokhtari, A., and Mahdavi, M. Federated learning with compression: Unified analysis and sharp guarantees. In *Proceedings of The 24th International Conference on Artificial Intelligence and Statistics*, volume 130 of *Proceedings of Machine Learning Research*, pp. 2350–2358. PMLR, 13–15 Apr 2021.

He, L., Karimireddy, S. P., and Jaggi, M. Byzantine-robust decentralized learning via clippedgossip. *arXiv preprint arXiv:2202.01545*, 2022.

Konečný, J., McMahan, H. B., Yu, F. X., Richtarik, P., Suresh, A. T., and Bacon, D. Federated learning: Strategies for improving communication efficiency. In *NIPS Workshop on Private Multi-Party Machine Learning*, 2016.

Lian, X., Zhang, C., Zhang, H., Hsieh, C.-J., Zhang, W., and Liu, J. Can decentralized algorithms outperform centralized algorithms? a case study for decentralized parallel stochastic gradient descent. In *Advances in Neural Information Processing Systems*, volume 30. Curran Associates, Inc., 2017.

Long, A. Protocol learning, decentralized frontier risk and the no-off problem. *arXiv preprint arXiv:2412.07890*, 2024.

Martínez Beltrán, E. T., Pérez, M. Q., Sánchez, P. M. S., Bernal, S. L., Bovet, G., Pérez, M. G., Pérez, G. M., and Celadrán, A. H. Decentralized federated learning: Fundamentals, state of the art, frameworks, trends, and challenges. *IEEE Communications Surveys & Tutorials*, 25(4):2983–3013, 2023.

McMahan, B., Moore, E., Ramage, D., Hampson, S., and Arcas, B. A. y. Communication-Efficient Learning of Deep Networks from Decentralized Data. In *Proceedings of the 20th International Conference on Artificial Intelligence and Statistics*, volume 54 of *Proceedings of Machine Learning Research*, pp. 1273–1282. PMLR, 20–22 Apr 2017.

Muñoz González, L., Biggio, B., Demontis, A., Paudice, A., Wongrassamee, V., Lupu, E. C., and Roli, F. Towards poisoning of deep learning algorithms with back-gradient optimization. In *Proceedings of the 10th ACM Workshop on Artificial Intelligence and Security*, AISec ’17, pp. 27–38. Association for Computing Machinery, 2017.

Pillutla, K., Kakade, S. M., and Harchaoui, Z. Robust aggregation for federated learning. *IEEE Transactions on Signal Processing*, 70:1142–1154, 2022.

Rothchild, D., Panda, A., Ullah, E., Ivkin, N., Stoica, I., Braverman, V., Gonzalez, J., and Arora, R. FetchSGD: Communication-efficient federated learning with sketching. In *Proceedings of the 37th International Conference on Machine Learning*, volume 119 of *Proceedings of Machine Learning Research*, pp. 8253–8265. PMLR, 13–18 Jul 2020.

Sattler, F., Wiedemann, S., Müller, K.-R., and Samek, W. Robust and communication-efficient federated learning from non-i.i.d. data. *IEEE Transactions on Neural Networks and Learning Systems*, 31(9):3400–3413, 2020.

Shejwalkar, V. and Houmansadr, A. Manipulating the byzantine: Optimizing model poisoning attacks and defenses for federated learning. In *NDSS*, 2021.

Stich, S. U., Cordonnier, J.-B., and Jaggi, M. Sparsified sgd with memory. In *Advances in Neural Information Processing Systems*, volume 31. Curran Associates, Inc., 2018.

Sun, P., Liu, X., Wang, Z., and Liu, B. Byzantine-robust decentralized federated learning via dual-domain clustering and trust bootstrapping. In *Proceedings of the IEEE/CVF Conference on Computer Vision and Pattern Recognition (CVPR)*, pp. 24756–24765, June 2024.

Wang, T., Zheng, Z., and Lin, F. Federated learning framework based on trimmed mean aggregation rules. *Expert Systems with Applications*, 270:126354, 2025. ISSN 0957-4174.

Xie, C., Koyejo, O., and Gupta, I. Fall of empires: Breaking byzantine-tolerant sgd by inner product manipulation. In *Proceedings of The 35th Uncertainty in Artificial Intelligence Conference*, volume 115 of *Proceedings of Machine Learning Research*, pp. 261–270. PMLR, 22–25 Jul 2020.

Yin, D., Chen, Y., Kannan, R., and Bartlett, P. Byzantine-robust distributed learning: Towards optimal statistical rates. In *Proceedings of the 35th International Conference on Machine Learning*, volume 80 of *Proceedings of Machine Learning Research*, pp. 5650–5659. PMLR, 10–15 Jul 2018.

A. Proof of Theorem 4.7

We provide a detailed proof of the convergence guarantee for SKETCHGUARD under strongly convex objectives with sketch-based compression. The proof structure follows the analysis framework of BALANCE (Fang et al., 2024), with key modifications to handle Count Sketch compression errors through the effective threshold parameter γ_{eff} .

A.1. Setup and Notation

We denote by $\mathbf{g}(\mathbf{w}_i^t)$ the stochastic gradient computed by client i at round t . The local update is:

$$\mathbf{w}_i^{t+1/2} = \mathbf{w}_i^t - \eta \mathbf{g}(\mathbf{w}_i^t), \quad (10)$$

where $\eta > 0$ is the learning rate. For simplicity in the proof, we drop the superscript t in \mathcal{S}_i^t and write \mathcal{S}_i .

A.2. Model Update Analysis

The model update for client i can be expressed as:

$$\begin{aligned} \mathbf{w}_i^{t+1} - \mathbf{w}_i^t &= \alpha \mathbf{w}_i^{t+1/2} \\ &\quad + (1 - \alpha) \frac{1}{|\mathcal{S}_i|} \sum_{j \in \mathcal{S}_i} \mathbf{w}_j^{t+1/2} - \mathbf{w}_i^t \end{aligned} \quad (11)$$

$$\begin{aligned} &= \alpha \mathbf{w}_i^{t+1/2} + (1 - \alpha) \frac{1}{|\mathcal{S}_i|} \\ &\quad \times \sum_{j \in \mathcal{S}_i} (\mathbf{w}_j^{t+1/2} - \mathbf{w}_i^{t+1/2} + \mathbf{w}_i^{t+1/2}) - \mathbf{w}_i^t \end{aligned} \quad (12)$$

$$\begin{aligned} &= \mathbf{w}_i^{t+1/2} + \frac{1 - \alpha}{|\mathcal{S}_i|} \\ &\quad \times \sum_{j \in \mathcal{S}_i} (\mathbf{w}_j^{t+1/2} - \mathbf{w}_i^{t+1/2}) - \mathbf{w}_i^t \end{aligned} \quad (13)$$

$$\begin{aligned} &= -\eta \mathbf{g}(\mathbf{w}_i^t) + \frac{1 - \alpha}{|\mathcal{S}_i|} \\ &\quad \times \sum_{j \in \mathcal{S}_i} (\mathbf{w}_j^{t+1/2} - \mathbf{w}_i^{t+1/2}) \end{aligned} \quad (14)$$

A.3. Applying Smoothness

By the L -smoothness assumption, we have:

$$\begin{aligned} F(\mathbf{w}_i^{t+1}) &\leq F(\mathbf{w}_i^t) + \langle \nabla F(\mathbf{w}_i^t), \mathbf{w}_i^{t+1} - \mathbf{w}_i^t \rangle \\ &\quad + \frac{L}{2} \|\mathbf{w}_i^{t+1} - \mathbf{w}_i^t\|^2 \end{aligned} \quad (15)$$

Substituting the model update expression:

$$\begin{aligned}
 F(\mathbf{w}_i^{t+1}) &\leq F(\mathbf{w}_i^t) - \eta \langle \nabla F(\mathbf{w}_i^t), \mathbf{g}(\mathbf{w}_i^t) \rangle \\
 &\quad + \langle \nabla F(\mathbf{w}_i^t), \frac{1-\alpha}{|\mathcal{S}_i|} \sum_{j \in \mathcal{S}_i} (\mathbf{w}_j^{t+1/2} - \mathbf{w}_i^{t+1/2}) \rangle \\
 &\quad + \frac{L}{2} \left\| -\eta \mathbf{g}(\mathbf{w}_i^t) \right. \\
 &\quad \left. + \frac{1-\alpha}{|\mathcal{S}_i|} \sum_{j \in \mathcal{S}_i} (\mathbf{w}_j^{t+1/2} - \mathbf{w}_i^{t+1/2}) \right\|^2
 \end{aligned} \tag{16}$$

A.4. Bounding the Quadratic Term

Using the inequality $\|a + b\|^2 \leq 2\|a\|^2 + 2\|b\|^2$:

$$\begin{aligned}
 &\left\| -\eta \mathbf{g}(\mathbf{w}_i^t) + \frac{1-\alpha}{|\mathcal{S}_i|} \sum_{j \in \mathcal{S}_i} (\mathbf{w}_j^{t+1/2} - \mathbf{w}_i^{t+1/2}) \right\|^2 \\
 &\leq 2\eta^2 \|\mathbf{g}(\mathbf{w}_i^t)\|^2 \\
 &\quad + 2 \left\| \frac{1-\alpha}{|\mathcal{S}_i|} \sum_{j \in \mathcal{S}_i} (\mathbf{w}_j^{t+1/2} - \mathbf{w}_i^{t+1/2}) \right\|^2
 \end{aligned} \tag{17}$$

A.5. Impact of Sketch-Based Filtering

With sketch-based filtering, neighbor j is accepted if:

$$\begin{aligned}
 &\|\text{CS}(\mathbf{w}_i^{t+1/2}) - \text{CS}(\mathbf{w}_j^{t+1/2})\| \\
 &\leq \gamma \exp(-\kappa t/T) \|\text{CS}(\mathbf{w}_i^{t+1/2})\|
 \end{aligned} \tag{18}$$

By the distance preservation property of Count Sketch (Charikar et al., 2002), this implies:

$$\begin{aligned}
 &\|\mathbf{w}_i^{t+1/2} - \mathbf{w}_j^{t+1/2}\| \\
 &\leq \gamma \sqrt{\frac{1+\epsilon}{1-\epsilon}} \exp(-\kappa t/T) \|\mathbf{w}_i^{t+1/2}\|
 \end{aligned} \tag{19}$$

Define $\gamma_{\text{eff}} = \gamma \sqrt{(1+\epsilon)/(1-\epsilon)}$. Then:

$$\left\| \frac{1}{|\mathcal{S}_i|} \sum_{j \in \mathcal{S}_i} (\mathbf{w}_j^{t+1/2} - \mathbf{w}_i^{t+1/2}) \right\| \leq \gamma_{\text{eff}} \psi \tag{20}$$

where we used the bounded parameters assumption that $\|\mathbf{w}_i^{t+1/2}\| \leq \psi$.

A.6. Taking Expectation

Taking expectation and using the bounded variance assumption:

$$\begin{aligned}
 \mathbb{E}[F(\mathbf{w}_i^{t+1})] &\leq \mathbb{E}[F(\mathbf{w}_i^t)] - \eta \|\nabla F(\mathbf{w}_i^t)\|^2 \\
 &\quad + (1-\alpha)\gamma_{\text{eff}}\psi\rho \\
 &\quad + L\eta^2(\|\nabla F(\mathbf{w}_i^t)\|^2 + \delta^2) \\
 &\quad + L(1-\alpha)^2\gamma_{\text{eff}}^2\psi^2
 \end{aligned} \tag{21}$$

A.7. Simplifying with Parameter Constraints

With $\eta \leq 1/(4L)$, we have $L\eta^2 \leq \eta/4$:

$$\begin{aligned}\mathbb{E}[F(\mathbf{w}_i^{t+1})] &\leq \mathbb{E}[F(\mathbf{w}_i^t)] - \frac{\eta}{2} \|\nabla F(\mathbf{w}_i^t)\|^2 \\ &\quad + L\eta^2\delta^2 + 2\gamma_{\text{eff}}\psi\rho(1-\alpha)\end{aligned}\tag{22}$$

where we chose $\gamma_{\text{eff}} \leq \rho/(L\psi(1-\alpha))$.

A.8. Applying Strong Convexity

By the strong convexity assumption and the Polyak-Łojasiewicz inequality:

$$\|\nabla F(\mathbf{w}_i^t)\|^2 \geq 2\mu(F(\mathbf{w}_i^t) - F(\mathbf{w}^*))\tag{23}$$

Therefore:

$$\begin{aligned}\mathbb{E}[F(\mathbf{w}_i^{t+1}) - F(\mathbf{w}^*)] &\leq (1-\mu\eta)\mathbb{E}[F(\mathbf{w}_i^t) - F(\mathbf{w}^*)] \\ &\quad + L\eta^2\delta^2 + 2\gamma_{\text{eff}}\psi\rho(1-\alpha)\end{aligned}\tag{24}$$

A.9. Telescoping and Final Bound

Telescoping over $t = 0, 1, \dots, T-1$:

$$\begin{aligned}\mathbb{E}[F(\mathbf{w}_i^T) - F(\mathbf{w}^*)] &\leq (1-\mu\eta)^T[F(\mathbf{w}_i^0) - F(\mathbf{w}^*)] \\ &\quad + \sum_{t=0}^{T-1} (1-\mu\eta)^{T-1-t} \\ &\quad \times (L\eta^2\delta^2 + 2\gamma_{\text{eff}}\psi\rho(1-\alpha)) \\ &= (1-\mu\eta)^T[F(\mathbf{w}_i^0) - F(\mathbf{w}^*)] \\ &\quad + \frac{1 - (1-\mu\eta)^T}{\mu\eta} \\ &\quad \times (L\eta^2\delta^2 + 2\gamma_{\text{eff}}\psi\rho(1-\alpha)) \\ &\leq (1-\mu\eta)^T[F(\mathbf{w}_i^0) - F(\mathbf{w}^*)] \\ &\quad + \frac{2L\eta\delta^2}{\mu} + \frac{2\gamma_{\text{eff}}\rho\psi(1-\alpha)}{\mu\eta}\end{aligned}\tag{25}$$

This completes the proof of Theorem 4.7. The key observation is that the compression error only affects the convergence through $\gamma_{\text{eff}} = \gamma\sqrt{(1+\epsilon)/(1-\epsilon)}$, introducing a controllable degradation factor while maintaining the same convergence rate as the state-of-the-art.

B. Proof of Theorem 4.8

We establish the convergence guarantee for SKETCHGUARD in non-convex settings, adapting the BALANCE analysis framework (Fang et al., 2024) for sketch compression.

B.1. Starting from Smoothness

Following the analysis from Appendix A up to the expectation bound, we have:

$$\begin{aligned}\mathbb{E}[F(\mathbf{w}_i^{t+1})] &\leq \mathbb{E}[F(\mathbf{w}_i^t)] - \frac{\eta}{2} \|\nabla F(\mathbf{w}_i^t)\|^2 \\ &\quad + 2L\eta^2\delta^2 + 2\gamma_{\text{eff}}\psi\rho(1-\alpha)\end{aligned}\tag{26}$$

B.2. Rearranging for Gradient Norm

Rearranging the inequality:

$$\begin{aligned}
 & \frac{\eta}{2} \mathbb{E}[\|\nabla F(\mathbf{w}_i^t)\|^2] \\
 & \leq \mathbb{E}[F(\mathbf{w}_i^t) - F(\mathbf{w}_i^{t+1})] \\
 & \quad + 2L\eta^2\delta^2 + 2\gamma_{\text{eff}}\psi\rho(1 - \alpha)
 \end{aligned} \tag{27}$$

B.3. Telescoping

Summing from $t = 0$ to $T - 1$:

$$\begin{aligned}
 & \frac{\eta}{2} \sum_{t=0}^{T-1} \mathbb{E}[\|\nabla F(\mathbf{w}_i^t)\|^2] \\
 & \leq F(\mathbf{w}_i^0) - \mathbb{E}[F(\mathbf{w}_i^T)] \\
 & \quad + T(2L\eta^2\delta^2 + 2\gamma_{\text{eff}}\psi\rho(1 - \alpha))
 \end{aligned} \tag{28}$$

B.4. Averaging and Using Lower Bound

Since $F(\mathbf{w}_i^T) \geq F^*$:

$$\begin{aligned}
 & \frac{1}{T} \sum_{t=0}^{T-1} \mathbb{E}[\|\nabla F(\mathbf{w}_i^t)\|^2] \\
 & \leq \frac{2(F(\mathbf{w}_i^0) - F^*)}{\eta T} \\
 & \quad + 4L\eta\delta^2 + \frac{4\gamma_{\text{eff}}\psi\rho(1 - \alpha)}{\eta}
 \end{aligned} \tag{29}$$

This establishes Theorem 4.8. The convergence rate matches the optimal rate for non-convex optimization, with the compression error appearing only through γ_{eff} .

C. Comparison with Existing Methods

Table 3 compares SKETCHGUARD with existing Byzantine-robust DFL algorithms across key properties. SKETCHGUARD is the only method that combines convergence guarantees in both convex and non-convex settings, operates without requiring knowledge of the compromised node ratio or complete graph assumptions, and achieves high scalability through sketch-based compression.

Table 3. Comparison of Byzantine-robust decentralized aggregation algorithms. "Convex"/"Non-convex" indicate convergence guarantees; "No c_i " means no need to know compromised node ratio; "No Complete" means no complete-graph assumption.

Algorithm	Convex	Non-convex	No c_i	No Complete	Scalable
UBAR (Guo et al., 2022)	—	—	—	—	Med.
LEARN (El-Mhamdi et al., 2021)	—	✓	—	—	Low
SCCLIP (He et al., 2022)	—	✓	✓	✓	Med.
BALANCE (Fang et al., 2024)	✓	✓	✓	✓	Med.
WFAGG (Cajaraville-Aboy et al., 2025)	—	—	✓	✓	Med.
SKETCHGUARD	✓	✓	✓	✓	High

D. Supplementary Experimental Details

This appendix provides comprehensive details about the experimental setup, including model architectures, hyperparameter configurations, network topologies, attack configurations, and scalability experiment specifications used throughout our study.

D.1. Detailed Model Architectures

We provide complete architectural specifications for the three datasets used in our experiments: FEMNIST, CelebA, and Sent140. The image-based models (FEMNIST and CelebA) follow standard convolutional designs, while Sent140 uses an LSTM-based architecture for sequential text data.

D.1.1. FEMNIST ARCHITECTURE

The FEMNIST model follows the original LEAF specification with a convolutional neural network design. The architecture consists of two convolutional layers followed by max pooling and two fully connected layers. Table 4 provides the complete layer-by-layer specification, including parameter counts and output dimensions.

Table 4. FEMNIST Model Architecture Details

Layer	Type	Parameters	Output Size
Input	—	—	$1 \times 28 \times 28$
Conv1	Conv2d	$32 \times (5 \times 5 \times 1) + 32$	$32 \times 28 \times 28$
Pool1	MaxPool2d	—	$32 \times 14 \times 14$
Conv2	Conv2d	$64 \times (5 \times 5 \times 32) + 64$	$64 \times 14 \times 14$
Pool2	MaxPool2d	—	$64 \times 7 \times 7$
Flatten	—	—	3136
FC1	Linear	$3136 \times 2048 + 2048$	2048
FC2	Linear	$2048 \times 62 + 62$	62
Total		6,603,710	

D.1.2. CELEBA ARCHITECTURE

The CelebA model uses a LeNet-style architecture adapted for larger RGB input images (84×84 pixels). The network has a similar structure to FEMNIST but with modified convolutional layers to handle color images and a binary classification output. The complete architecture is detailed in Table 5.

Table 5. CelebA Model Architecture Details

Layer	Type	Parameters	Output Size
Input	—	—	$3 \times 84 \times 84$
Conv1	Conv2d	$30 \times (3 \times 3 \times 3) + 30$	$30 \times 84 \times 84$
Pool1	MaxPool2d	—	$30 \times 42 \times 42$
Conv2	Conv2d	$50 \times (3 \times 3 \times 30) + 50$	$50 \times 42 \times 42$
Pool2	MaxPool2d	—	$50 \times 21 \times 21$
Flatten	—	—	22050
FC1	Linear	$22050 \times 100 + 100$	100
FC2	Linear	$100 \times 2 + 2$	2
Total		2,219,692	

D.1.3. SENT140 ARCHITECTURE

The Sent140 model uses a stacked LSTM architecture following the LEAF reference implementation. The model processes variable-length text sequences through an embedding layer, a 2-layer LSTM, and fully connected output layers. Table 6 provides the complete specification.

Table 6. Sent140 Model Architecture Details

Layer	Type	Configuration	Output Size
Input	–	–	seq_len
Embedding	Embedding	vocab=10000, dim=100	seq_len × 100
LSTM	Stacked LSTM	2 layers, hidden=100	100
Dropout	Dropout	$p = 0.1$	100
FC1	Linear	100 → 128	128
FC2	Linear	128 → 2	2
Total			~1.2M

The embedding layer maps vocabulary indices (size 10,000) to 100-dimensional dense vectors. The stacked 2-layer LSTM with 100 hidden units processes the embedded sequence with dropout for regularization. The final hidden state passes through two fully connected layers for binary sentiment classification.

D.2. Evaluation Metrics

We evaluate defense mechanisms using four complementary metrics that capture robustness, backdoor resilience, computational efficiency, and communication overhead.

Test Error Rate (TER). Defined as $1 - \text{test accuracy}$, TER measures performance degradation averaged across honest clients. Lower values indicate better Byzantine resilience against model poisoning attacks. TER is computed on each honest client’s local test set and averaged across all honest clients in the network.

Attack Success Rate (ASR). For backdoor attacks, ASR measures the fraction of triggered test samples classified as the attacker’s target label on honest client models. Lower ASR indicates better resilience to backdoor injection. The random-chance baseline is $\text{ASR} \approx 1/C$ where C is the number of classes: 1.6% for FEMNIST (62 classes) and 50% for CelebA and Sent140 (binary classification). ASR is computed by applying the backdoor trigger to clean test samples and measuring the fraction misclassified to the target label.

Per-Round Computation Time. Wall-clock time for neighbor screening and aggregation phases per client per round, excluding local training which remains constant across methods. This metric captures the computational overhead introduced by Byzantine-robust aggregation mechanisms. All timing measurements are recorded on identical hardware (CPU-only for reproducibility) and averaged across all clients and rounds.

Communication Overhead. Total parameters transmitted per client per round, including both sketches (for SKETCHGUARD) and full model exchanges. We report both absolute parameter counts and reduction percentages relative to full-precision baselines that transmit complete models to all neighbors.

D.3. Complete Experimental Configuration

This section details all hyperparameters and configuration settings used across our experiments to ensure reproducibility.

D.3.1. NETWORK TOPOLOGY SPECIFICATIONS

We evaluate defense mechanisms across five different network topologies representing varying levels of connectivity. The ring topology represents minimal connectivity (degree 2), while Erdős-Renyi graphs with varying connection probabilities p provide intermediate connectivity levels. The fully connected topology represents maximum connectivity where each node connects to all others. Table 7 specifies the parameters and expected node degrees for each topology in our 20-node experimental networks.

Table 7. Network Topology Configurations

Topology	Parameters	Expected Degree
Ring	–	2
Erdős-Rényi (sparse)	$p = 0.2$	3.8
Erdős-Rényi (medium)	$p = 0.45$	8.55
Erdős-Rényi (dense)	$p = 0.6$	11.4
Fully Connected	–	19

D.3.2. HYPERPARAMETER SETTINGS

Table 8 presents the complete set of hyperparameters used in our experiments, organized by category. Training configuration parameters were selected based on standard federated learning practices. Defense mechanism parameters (γ , κ , α) were tuned to balance robustness and model utility. For SKETCHGUARD, we set dataset-specific sketch sizes to achieve comparable compression ratios across different model dimensions.

Table 8. Complete Hyperparameter Configuration

Parameter	Value
<i>Training Configuration</i>	
Number of clients	20
Global rounds	10
Local epochs per round	3
Batch size	64
Learning rate	0.01 (FEMNIST, Sent140), 0.001 (CelebA)
Maximum samples per client	10,000 (FEMNIST), 4,500 (CelebA, Sent140)
Random seeds	987654321, 39573295, 32599368
<i>SketchGuard Parameters</i>	
Sketch size (k)	1,000 (FEMNIST), 350 (CelebA), 180 (Sent140)
Threshold parameter (γ)	2.0
Decay parameter (κ)	1.0
Mixing parameter (α)	0.5
Hash seed	42
<i>BALANCE Parameters</i>	
Threshold parameter (γ)	2.0
Decay parameter (κ)	1.0
Mixing parameter (α)	0.5
<i>UBAR Parameters</i>	
Robustness parameter (ρ)	1.0 – attack percentage
<i>KRUM Parameters</i>	
Compromised fraction	Attack percentage

D.3.3. BACKDOOR ATTACK CONFIGURATION

Table 9 details the backdoor attack configurations used for each dataset. For image datasets (FEMNIST and CelebA), the backdoor trigger consists of a white square pattern inserted in the bottom-right corner of the image. For Sent140, the trigger consists of rare vocabulary token indices appended to the end of the text sequence.

Table 9. Backdoor Attack Configuration by Dataset

Dataset	Target Label	Trigger Size	Trigger Type
FEMNIST	0	4×4 pixels	White square (bottom-right)
CelebA	0 (not smiling)	8×8 pixels	White square (bottom-right)
Sent140	1 (positive)	3 tokens	Rare word indices appended

For Sent140, the trigger tokens are selected from high vocabulary indices (9997, 9998, 9999) that rarely appear in natural

text, ensuring the trigger pattern is distinctive and unlikely to occur in benign samples.

D.4. Detailed Attack Descriptions

We evaluate Byzantine robustness using four representative attack strategies that span different threat models and sophistication levels.

D.4.1. DIRECTED DEVIATION ATTACK

Directed deviation attacks (Fang et al., 2020) employ an optimization-based approach that crafts malicious updates by solving for parameters that maximize deviation in the direction opposite to honest gradient descent. This adaptive attack strategy represents a strong adversary that actively attempts to subvert Byzantine-robust aggregation mechanisms by carefully positioning malicious updates to evade detection while maximizing impact. The attack computes the mean of honest updates and crafts malicious updates as:

$$\hat{\mathbf{w}}_j = \bar{\mathbf{w}} - \lambda \cdot \text{sign}(\bar{\mathbf{w}} - \mathbf{w}^t) \quad (30)$$

where $\bar{\mathbf{w}}$ is the mean honest update, \mathbf{w}^t is the current model, and λ controls attack intensity. This attack has demonstrated effectiveness against common Byzantine-robust aggregation rules including Krum and trimmed mean.

D.4.2. GAUSSIAN ATTACK

Gaussian attacks (Blanchard et al., 2017) inject random noise $\hat{\mathbf{w}}_j = \mathcal{N}(0, 200\mathbf{I})$, representing less sophisticated but realistic adversaries that disrupt convergence through stochastic perturbations. While simpler than directed deviation, these attacks model practical scenarios where attackers lack complete knowledge of the aggregation mechanism or resources for optimization-based attacks. The high variance ($\sigma^2 = 200$) ensures significant disruption to model convergence.

D.4.3. KRUM ATTACK

Krum attacks (Fang et al., 2020) craft malicious models that cause Krum to select the attacker’s chosen model. The attack works by:

1. Computing the mean of honest models as a reference
2. Creating a primary malicious model in the opposite direction of honest gradient descent
3. Creating supporting malicious models very close to the primary to minimize the Krum score of the primary model

The attack exploits Krum’s reliance on pairwise distances: if attackers control enough nodes, they can cluster their models tightly while being far from honest models, causing Krum to select the malicious model as it appears most “central.”

D.4.4. BACKDOOR ATTACK

Backdoor attacks (Bagdasaryan et al., 2020) represent a distinct threat model where adversaries aim to embed hidden functionality rather than degrade overall performance. Malicious clients augment their training data with trigger patterns mapped to an attacker-chosen target label, then scale their model updates by a factor proportional to the total number of clients to amplify the backdoor’s persistence during aggregation. Unlike other attacks that maximize test error, backdoor attacks preserve main task accuracy while causing misclassification only on triggered inputs, making them particularly stealthy. Dataset-specific trigger configurations are detailed in Table 9.

D.5. Scalability Experiments

We conducted two types of scalability experiments to evaluate how defense mechanisms perform under different scaling conditions: network size scaling and model dimensionality scaling.

D.5.1. NETWORK SIZE SCALING

To evaluate the computational scalability of defense mechanisms with respect to network size, we conducted experiments on k-regular graphs with varying numbers of participants. Table 10 shows the configurations used, with network sizes ranging

from 20 to 300 nodes. All networks maintain 50% Byzantine nodes to test defense robustness under high attack scenarios. The node degree was selected to ensure connectivity while maintaining realistic peer-to-peer network constraints. These experiments used shorter training runs (3 rounds with 1 local epoch each) to focus on measuring computational overhead rather than convergence behavior. All timing measurements were performed on CPU to ensure consistent and reproducible results across different hardware configurations.

Table 10. Network Size Scaling Configurations

Node Degree (k)	Network Size	Attack Percentage
16	20	50%
32	35	50%
96	100	50%
154	155	50%
299	300	50%

D.5.2. MODEL SCALING VARIANTS

To investigate the impact of model dimensionality on defense mechanism performance, we created five variants of the FEMNIST architecture with different parameter counts. Table 11 describes these variants, ranging from the Tiny model with approximately 220K parameters to the XLarge model with over 60M parameters. These variants were created by systematically scaling the number of convolutional filters and fully connected layer dimensions while maintaining the overall architectural structure.

Table 11. Model Scaling Variants

Variant	Architecture Modifications	Parameters
Tiny	Reduced filter counts and hidden units	220,318
Small	Standard configuration	848,382
Baseline	Baseline FEMNIST architecture	6,603,710
Large	Increased filter counts and hidden units	26,154,814
XLarge	Further increased dimensions	60,271,678

Model dimensionality scaling experiments use a fixed k-regular graph with node degree 154 (155 total nodes) to isolate the effect of model size from network topology effects.